This article has been accepted for publication in a future issue of this journal, but has not been fully edited. Content may change prior to final publication. Citation information: DOI 10.1109/JSEN.2018.2824349, IEEE Sensors Journal

Experimental study of a real-time and highly sensitive fiber-optic porous silicon temperature sensing probe

Raffaele Caroselli, David Martín Sánchez, Salvador Ponce Alcántara, Francisco Prats Quilez, Luis Torrijos Morán, Jaime García-Rupérez, *Senior Member, IEEE*

***Abstract*—We report the development of a temperature sensing probe created as a result of the combination of an optical fiber and a porous silicon microcavity (PSMC). After determining the physical parameters of the PSMC to achieve the required porous sensing structure, it was fabricated by electrochemically etching a silicon wafer. A 1 mm^2 PSMC piece was attached to the tip of an optical fiber so that temperature variations can be monitored in real-time exactly on that point. Firstly, the performance of the PSMC sensor probe was characterized in a stable environment as water, obtaining a sensitivity around 110 pm/ºC and a resolution in the 10^{-4} ºC range. Afterwards, the temperature transmission dynamics in air environment were studied.**

***Index Terms*— Fiber-optic sensor, porous silicon, Bragg reflector, microcavity, temperature monitoring**

I. Introduction

FIBER-OPTIC SENSORS (FOSs) have been widely studied and exploited becoming one of the principal optical sensing technologies [1]. Nowadays, FOSs are applied in several sensing applications such as for the measurement of refractive index, strain, temperature, pressure, vibration or bending [2]. This sensing versatility is due to the possibility of developing different types of FOSs where the selected parameter affects the intensity, frequency, polarization or phase of the light travelling through the fiber [3]. Furthermore, they offer several advantages including high sensitivity, immunity to electromagnetic interferences, small dimensions, cost effectiveness and the ability to operate in a wide range of environments [4]. One of the most important applications where FOSs have found a great success is temperature sensing [2, 5]. In fact, temperature is a crucial parameter in several fields, especially research laboratories, food industries, environmental monitoring, monitoring of biochemical reactions or military and aerospace uses [6, 7]. Presently, many FOS configurations can be found, the majority of which are based on fiber interferometers and on fiber Bragg gratings (FBGs) [1-3, 5, 8]. Despite most fiber-optic temperature sensors make use of the fiber itself as sensing element, this fact entails two main limitations. The first one consists in the relatively complex fabrication of the sensor, since the optical sensing structure has to be directly fabricated on the fiber itself. The second one is related with the thermal properties of the fiber-based sensors, namely, the thermo-optic coefficient (TOC), i.e., the variation of the refractive index (RI) as a function of the temperature, and the thermal diffusivity, i.e., the temperature transfer rate of the material. Since the optical fiber is made of silica, it is characterized by relatively low TOC and thermal diffusivity. A low TOC determines a low sensitivity towards temperature changes, whereas a low thermal diffusivity implies a larger time needed by the structure to reach the required temperature. As a matter of fact, regarding the temperature sensitivity, FBGs exhibit low values in the range of 10 pm/ºC [2, 9], since the sensitivity is determined mainly by the material of the FBG. Several techniques have been used to enhance the sensitivity and reduce the response time. Among them, a widely used technique is using a metal package for the FBGs, leading to a sensitivity in the range of 27 pm/ºC and a real-time response [10]. However, this process increases the complexity and the cost for the development of such a temperature sensor. An alternative to FBGs are fiber long period gratings. These sensors reach a sensitivity in the range of 100 pm/ºC, but their high bending sensitivity may give rise to variations of the spectral response not related with the temperature variations [11, 12]. Furthermore, this type of configuration also presents the limitation of a complex fabrication.

To overcome such limitations, novel configurations have been developed in the last years as a result of the combination of optical fibers with an additional optical sensing component. For example, Liu et al. reported a fiber-optic sensor based on a silicon Fabry-Pérot cavity fabricated by attaching a silicon pillar to the tip of a single-mode fiber [9]. This configuration presented an experimental sensitivity of 84.6 pm/ºC and a real-time response, due to the larger TOC and thermal diffusivity of the silicon.

Within this context, we propose in this work the development and the experimental study of a real-time and high resolution FOS based on its combination with a porous silicon microcavity (PSMC) and its application for temperature sensing. The use of a porous silicon (PS) structure

This work was supported by the European Commission under project H2020-644242 SAPHELY, by the Spanish government under projects TEC2013-49987-EXP BIOGATE and TEC2015-63838-C3-1-R OPTONANOSENS and by the Generalitat Valenciana under the Doctoral Scholarship GRISOLIAP/2014/109 granted to Raffaele Caroselli.

R. Caroselli, D. Martín, S. Ponce, F. Prats, L. Torrijos and J. García-Rupérez are with the Nanophotonics Technology Center (NTC), Universitat Politècnica de València, Valencia 46022, Spain (email: jaigarru@ntc.upv.es).

This article has been accepted for publication in a future issue of this journal, but has not been fully edited. Content may change prior to final publication. Citation information: DOI 10.1109/JSEN.2018.2824349, IEEE Sensors Journal

as sensing element is justified by the advantages provided by this material platform. Firstly, PS can be formed simply, quickly and inexpensively since it is the result of the electrochemical etching of a silicon substrate [13, 14]. Moreover, the porous configuration of PS is highly beneficial for sensing purposes since it allows the infiltration of the target substances to be analyzed [15-17]. Furthermore, such material platform can be used for the creation of a wide range of configurations of photonic structures for sensing applications. Typically, layer-based optical structures based on PS have been developed, as for example single layers, like Fabry-Perot (FP) filters [18, 19], multilayers, like Bragg reflectors (BRs) [20, 21], or optical microcavities (MCs) [22-24]. More recently, PS-based integrated photonic structures have also been proposed, as for example Mach-Zehnder interferometers [25] or ring resonators (RRs) [26, 27].

The design, fabrication and characterization of the PSMC-based sensing probe proposed in this work, as well as the experimental opto-thermal setup developed to perform the experiments, are described in section 2. In section 3, the results obtained for the temperature variation experiments are reported and discussed. First, experiments in water environment were carried in order to study the performance of the sensor. A sensitivity value around 110 pm/ºC and a resolution in the 10^{-4} ºC range were obtained. Then, experiments in air environment were carried out in order to compare the results with those obtained in water environment and study how the temperature increases affect to the noise. A level of noise higher than that achieved in water environment was observed and the real-time response of the sensor was demonstrated.

II. Material And Methods

A. Sensing mechanism

Our sensing structure consisted of an optical microcavity (MC) created between two Bragg reflectors. A Bragg reflector is a periodic structure formed by alternating layers of high (n_H) and low (n_L) refractive index (RI) that provides a reflectivity spectrum characterized by the presence of a photonic band gap (PBG) centered on the Bragg wavelength, λ_B. The thickness of the layers, d_H and d_L, satisfy the relation $2(n_H \cdot d_H + n_L \cdot d_L) = m \cdot \lambda_B$, where m is the order of the Bragg condition. The microcavity structure can be obtained by placing a $\lambda_B/2$ layer between two Bragg reflectors. The reflectivity spectrum of the MC is characterized by the presence of a narrow resonance peak inside the PBG, whose position depends on the RI and the thickness of the layers. Those two parameters will depend on the temperature, since the RI will change due to the thermo-optic effect and the thickness will vary due to the thermal expansion. So, temperature variations will be determined by monitoring the shift of the resonance position that is produced due to the variation of those parameters.

B. PSMC modelling

A model based on the Transfer Matrix Method (TMM) [28, 29] was used to determine the structure parameters n_H, n_L, d_H, and d_L in order to obtain a resonant peak located at 1550 nm. This model allows to calculate the transmission and the reflection spectra of a one-dimensional structure consisting of an arbitrary number of alternated porous silicon (PS) layers with different porosities and thicknesses. These spectra are obtained from the contribution of the transmitted and reflected waves produced at each boundary between two layers.

In our study, we considered that the MC was created using a n_L porous layer having a thickness of $2h_L$. Therefore, our PSMC consisted of two Bragg reflectors, BR1 and BR2, having the MC layer between them, as described by the sequence $[n_H, n_L]\times7$, n_H, $n_{L\text{-}MC}$, n_H, $[n_L, n_H]\times7$. A scheme of the PSMC structure is shown in Fig. 1(a). The refractive indices and the corresponding thicknesses obtained in the design process were n_H=1.70, n_L=1.40, d_H=228 nm and d_L=278 nm. The Bruggeman equation was considered to relate refractive indices and porosities [30]. In this respect, the theoretical porosities for the n_H and n_L layers were 65% and 77%, respectively. The calculated reflectance spectrum of the simulated structure is shown in Fig. 1(b).

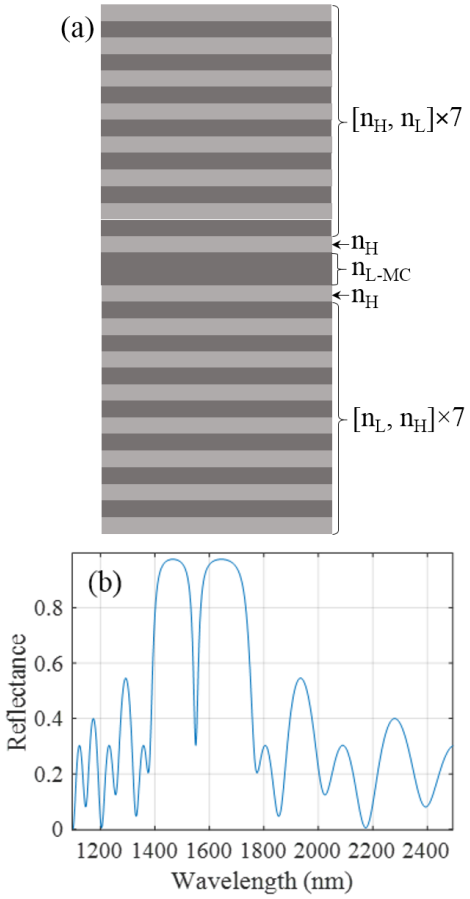

Fig. 1. (a) Scheme of the PSMC used in this work. (b) Simulated reflectance spectrum of the designed PSMC, having a cavity peak located at 1550 nm.

C. PSMC fabrication

The PSMC was fabricated by electrochemical etching a single side 20×20 mm^2 polished boron doped <100> oriented c-Si wafer, with electrical resistivity of 0.01–0.02 Ωcm. The Si wafer thickness was 725±15 µm. The solution used to produce the PS was composed by 48% hydrofluoric acid and

This article has been accepted for publication in a future issue of this journal, but has not been fully edited. Content may change prior to final publication. Citation information: DOI 10.1109/JSEN.2018.2824349, IEEE Sensors Journal

99% ethanol, in a 1:2 volume. Before the etching process, the silicon wafer was cleaned by using a piranha solution (volume ratio H_2SO_4:H_2O_2 = 3:1) at room temperature, to remove possible organic residues in the surface. Afterwards, the wafer was rinsed with deionized water. In order to remove residual surface impurities after the etching process, the wafer was cleaned with acetone and isopropyl alcohol, and rinsed in deionized water. The most important parameters to be taken into account associated to the etching process, carried out at room temperature, were the HF concentration [HF], the current density D, and the etching time T, as summarized in Table I. In order to obtain the layered structure, the current density was alternated between two values during the electrochemical etching process, 16 and 45 mA/cm^2, in order to obtain the two different porosities corresponding to the n_H and n_L layers. The wafer etched area had a diameter of 11 mm. The total time required for the creation of the PSMC structure was just around 4 minutes.

TABLE I
ELECTROCHEMICAL ETCHING PROTOCOL USED TO PREPARE THE PSMC

Layer	[HF]	J (mA/cm^2)	T(s)
n_H	16%	16	10.3
n_L	16%	45	6.9

D. PSMC physical and optical characterization

Figure 2(a) shows a scanning electron microscope (SEM) cross-sectional image of the fabricated PSMC, where the light and dark grey layers are the n_H and the n_L layers, respectively. The thicknesses measured with SEM of the n_H and n_L the layers were 215 nm and 265 nm, respectively. The overall thickness of PSMC was 7680 nm. The experimental RIs of the layers were obtained by adjusting the FTIR (Fourier transform infrared) reflectance spectrum of the PSMC, which is shown in Figure 2(b), with a mathematical model based on the TMM. The estimated values are n_H=1.92 and n_L=1.42, whereas the relative porosities were 57% and 75%, respectively. Such experimental results are in a good agreement with those calculated in the design stage. As it can be observed, the spectrum presents a resonance peak in 1566 nm, very close to the position expected from the design stage. The positive outcome of the PSMC spectrum was due to the correct configuration of the calculated etching process parameters.

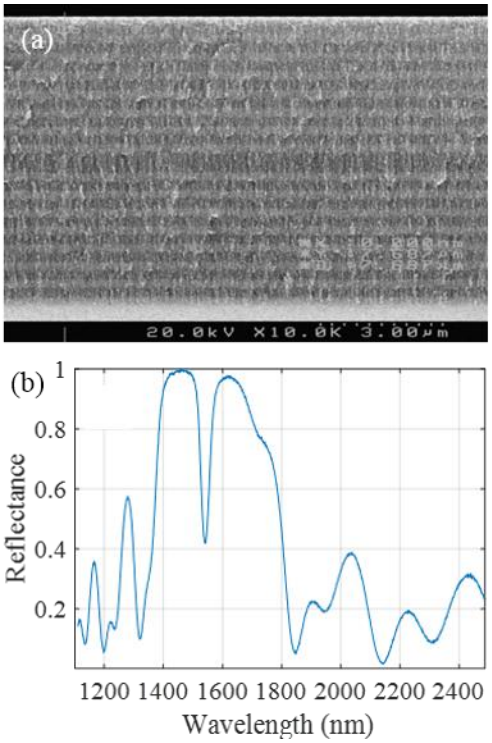

Fig. 2. (a) SEM cross-sectional image and (b) FTIR reflectance spectrum of the fabricated PSMC sample.

E. PSMC sensing probe preparation

The preparation of the PSMC sensing probe is schematically shown in Fig. 3. Firstly, the PSMC sample created by electrochemical etching was diced into square pieces of size 1 mm^2 by using a DAD3350 Disco automatic dicing saw. This small size will allow us to measure the temperature variations at a very specific point. The dicing process required around 6 minutes. In this way, considering the electrochemical etching and the dicing processes, around 90 PSMC sensors were obtained in 10 minutes. One of these square pieces was selected and attached to the tip of an optical fiber connector with the porous side facing it. To this aim, epoxy glue was used since it is transparent at 1550 nm.

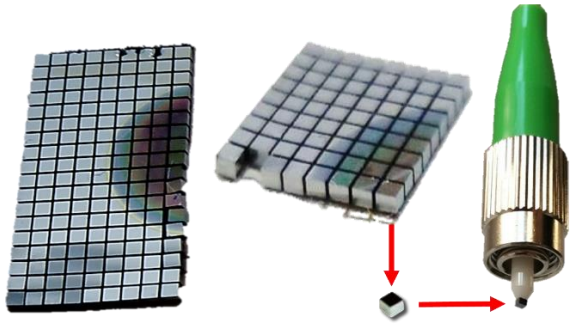

Fig. 3 Illustration of the development of the PSMC sensing probe.

F. Experimental setup and procedure

An opto-thermal setup was developed to carry out our experimental measurements. Such setup was composed by an optical part and a thermal part, which can operate at the same time, in order to change the temperature of the system and simultaneously monitor the spectrum evolution. Figure 4

This article has been accepted for publication in a future issue of this journal, but has not been fully edited. Content may change prior to final publication. Citation information: DOI 10.1109/JSEN.2018.2824349, IEEE Sensors Journal

shows a schematic illustration of the experimental setup. The PSMC sensing probe was connected to a National Instruments PXIe-4844 optical interrogator in order to acquire its reflectance spectrum. Such optical interrogator is an optical measuring apparatus able to obtain one spectrum every 0.1 seconds in a wavelength range of 1510-1590 nm with a resolution of 4 pm. This apparatus provides the advantage of analysing the reflected light spectrum in real-time. A LabVIEW program was developed to examine the evolution of the reflectance spectrum. More in detail, a Lorentzian fitting of the spectrum was implemented in order to enhance the accuracy of the resonance peak tracking.

Concerning the thermal setup, a Peltier cell was used as heater (or cooler). In order to control the Peltier cell, a LDC-3744C Precision Laser Diode Controller was used as temperature controller (TC). Finally, a thermocouple was used as temperature sensor to close the loop of the instrument internal controller. Using thermal paste, the Peltier cell and the thermocouple were attached and thermally connected to a heatsink. The Peltier cell heated or cooled the heatsink until the thermocouple reached the input temperature. In order to know the temperature being perceived by the PSMC sensing probe, a metallic stick temperature sensor was used as reference sensor.

Two different configurations were considered to detect temperature changes, first in water and then in air environment. In the sensing-in-water configuration, the PSMC sensing probe was immersed in a water-filled beaker. This beaker was placed on the heatsink where it was thermally connected with thermal paste. In the sensing-in-air configuration, the sensing probe was placed above the heatsink, close to the thermocouple, at a distance of 2 mm.

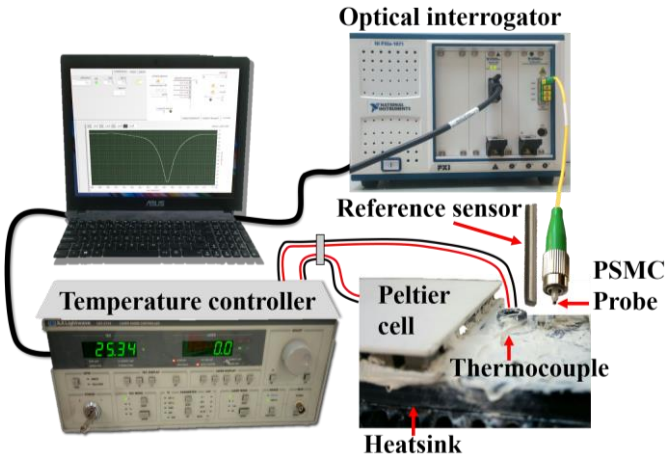

Fig. 4. Illustration of the opto-thermal setup used in the experiments.

III. Results and Discussions

A. Thermal setup performances analysis

Before carrying out the temperature sensing experiments with the sensing probe, the performances of the thermal setup were studied. As shown in Fig. 5, the TC input temperature was increased from 24 ºC to 25 ºC and the temperature perceived by the thermocouple was monitored in real-time and in-continuum. The average observed noise was $6 \cdot 10^{-3}$ ºC. Such noise was produced by the constant correction of the TC to keep the temperature at the input value. The time needed by the thermocouple to reach the increment of 1 ºC was around 30 seconds. This value represents the time needed by the Peltier cell to heat the heatsink and thus the thermocouple.

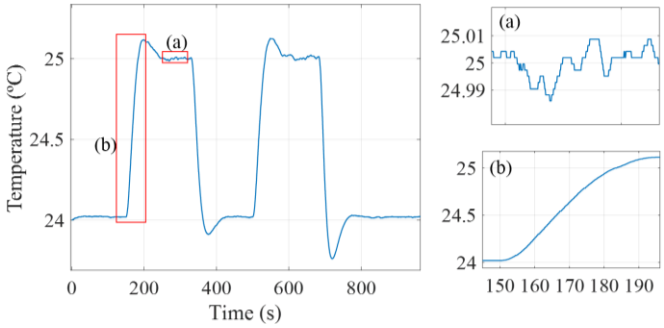

Fig. 5. Time evolution of the temperature perceived by the thermocouple. The inset (a) depicts the noise of the system, whereas the inset (b) depicts its response time.

B. Water environment experiments

Since water provides a more thermally stable system than air, experiments in water environment were carried out first, in order to characterize the sensitivity and the resolution of our PSMC sensing probe. The experiments were performed by constantly controlling the heatsink temperature and its variation in a degree-by-degree basis. At the same time, the evolution of the temperature perceived by the reference sensor was monitored in real-time. The evolution of the PSMC resonance peak was monitored in real-time.

The temperature changes applied to the heatsink were from 24 ºC to 25 ºC, from 26 ºC to 27 ºC, from 28 ºC to 29 ºC and from 30 ºC to 31 ºC. As a result of each temperature change, a temperature variation of 0.2 ºC was measured by the reference sensor; so, that will be the temperature variation being really measured by the PSMC sensing probe (i.e., not the 1ºC variation applied to the heatsink). Figure 6 shows the PSMC resonance peak time evolution relative to the temperature changes previously indicated, whereas Fig. 7 depicts the wavelength shift obtained for that 0.2 ºC variation depending on the initial heatsink temperature. A resonance peak shift of 22±1 pm was observed in all the cases for the temperature change of 0.2 ºC that was measured by the metallic reference sensor, thus leading to a sensitivity of 110±5 pm/ºC of the PSMC sensing probe. The average measured experimental noise was 0.6 pm, what considering the sensitivity of our sensor, corresponds to a temperature resolution of $6 \cdot 10^{-3}$ ºC. That was the noise level previously measured for the TC, what indicates that the measured resolution for the PSMC sensing probe is being limited by the thermal setup performance and it will probably be higher. Such results demonstrate that our PSMC temperature sensing probe was able to measure very small temperature variations at a very specific point. Note also that the noise level can be further reduced by around an order of magnitude by using a Discrete Fourier Transform (DFT) filtering algorithm in order to eliminate the high frequency components not related with the sensing (see Fig. 6). Thanks to such noise reduction process, a noise value of 0.07 pm was calculated, what leads to a temperature resolution of $6.3 \cdot 10^{-4}$

ºC.

Finally, note that the time required to reach the plateau for each temperature change (around 90 seconds) is determined by, firstly, the time needed by the Peltier cell to reach the required temperature and, then, by the time needed by the water environment to achieve such temperature. This means that water took around 60 seconds to reach the required temperature. As a matter of fact, in this case, water acted like a second heatsink: as the heatsink warmed up and transferred the heat to the thermocouple, the water warmed up and transfer the heat to the sensing probe.

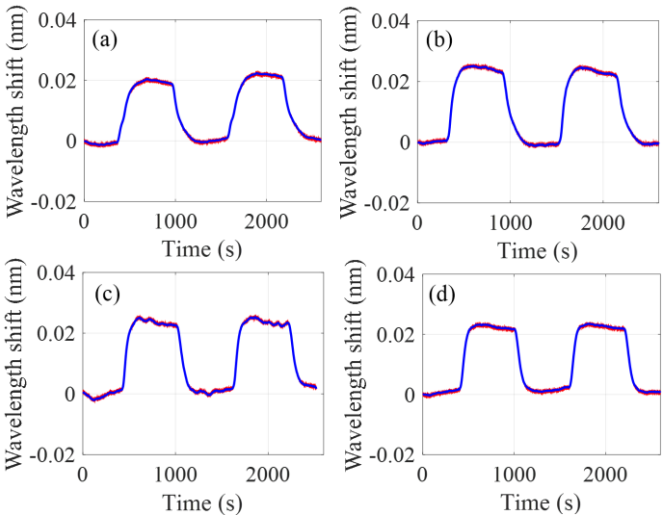

Fig. 6. Resonance peak time evolutions of the PSMC sensing probe relative to the heatsink temperature change (a) from 24ºC to 25ºC, (b) from 26ºC to 27ºC, (c) from 28ºC to 29ºC and (d) from 30ºC to 31ºC. Note that these 1ºC changes of the heatsink correspond to a 0.2ºC change in the sensor position. The experimental evolution is represented in red, whereas the evolution after the noise filtering process is represented in blue.

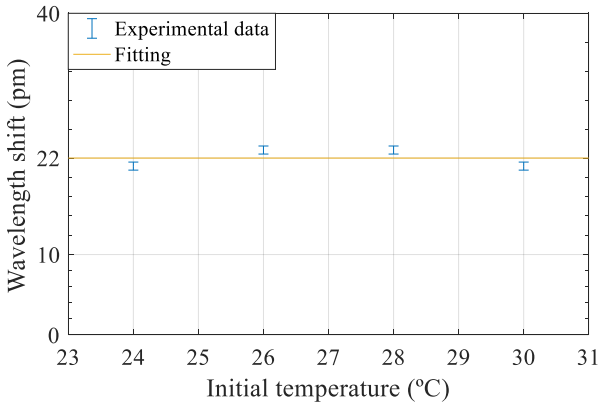

Fig. 7: Relationship between the resonance wavelength shift obtained for a 0.2 ºC temperature variation and the initial heatsink temperature value used in the water environment experiments.

C. *Air environment experiments*

Once the PSMC sensing probe performance was characterized using water environment, experiments in air environment were carried out. The temperature changes applied to the heatsink were from 23 ºC to 24 ºC, from 24 ºC to 25 ºC, from 26 ºC to 27 ºC and from 28 ºC to 29 ºC. Figure 8 shows the PSMC resonance peak time evolutions relative to these temperature changes. Analyzing the evolutions, it is possible to observe that the average value of the noise was considerably higher than that observed in water environment experiments. Moreover, the noise increased for higher initial temperature values. In Table II, the noise values of the experiments in air environment are reported and confirm what is observed in Fig. 8. The higher level of noise was due to the perturbations produced by the air environment, which is a less stable system than water. The air environment constantly tries to take the system to the room temperature, as shown in Fig. 9. As it is known, the farthest from the room temperature is the temperature perceived by the sensing probe the largest is the interference produced by the environment. This means that when the temperature perceived by the sensing probe is close to the room temperature, the influence of the environment is low. Otherwise, when temperature perceived by the sensing probe is far from the room temperature, the influence of the environment is larger, affecting the experimental signal evolution and thus producing a high level of noise.

Finally, the average time needed to reach the plateau is around 30 seconds, the same time needed by the thermal setup itself to heat up the thermocouple. Such results demonstrate that our temperature sensing probe was able to measure very small temperature variations in real-time.

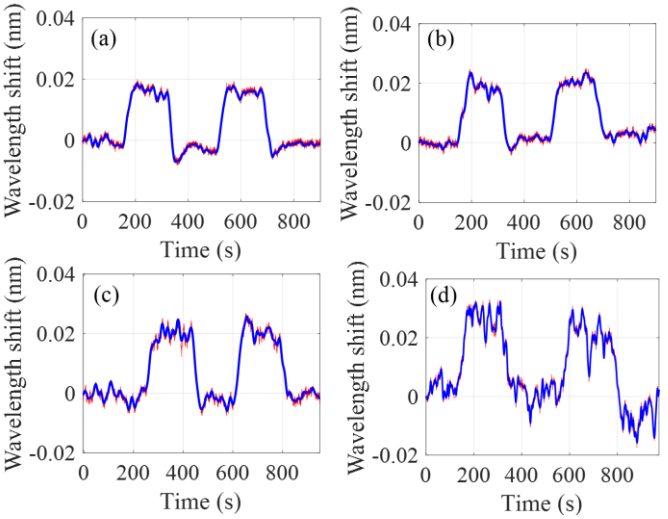

Fig. 8. Resonance peak time evolutions of the PSMC sensing probe relative to the heatsink temperature change (a) from 23ºC to 24ºC, (b) from 24ºC to 25ºC, (c) from 26ºC to 27ºC and (d) from 28ºC to 29ºC. Note that these 1ºC changes of the heatsink correspond to a 0.2ºC change in the sensor position. The experimental evolution is represented in red, while the evolution after a noise filtering process is represented in blue.

TABLE II
VALUE OF THE NOISE OF THE AIR EXPERIMENTS

Temperature change (ºC)	Noise (pm)
23-24	1.1
24-25	1.4
26-27	2.1
28-29	3.4

This article has been accepted for publication in a future issue of this journal, but has not been fully edited. Content may change prior to final publication. Citation information: DOI 10.1109/JSEN.2018.2824349, IEEE Sensors Journal

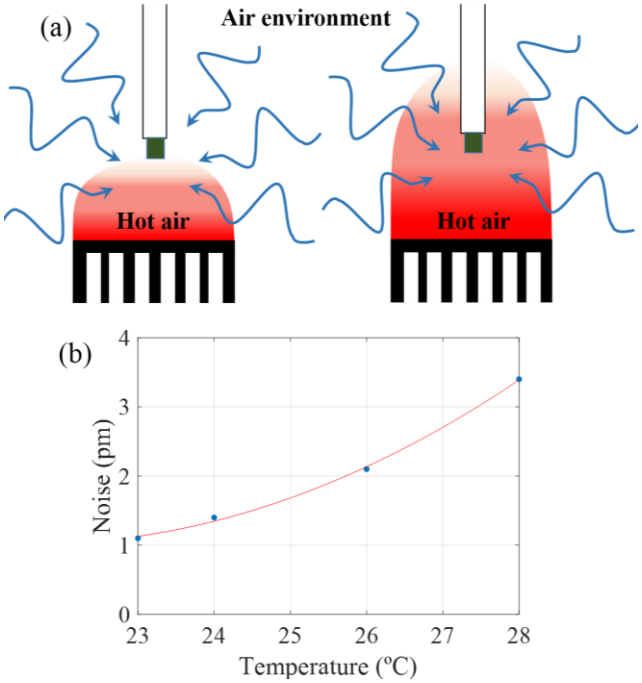

Fig. 9. (a) Schematic illustration of the environment thermal influence on the sensing-in-air configuration system. (b) Relationship between the measured noise with the initial heatsink temperature value used in the air environment experiments.

IV. Conclusions

In this paper, we reported the development and the experimental study of a real-time and highly sensitive temperature sensing probe based on the combination of an optical fiber and a PSMC. The PSMC sensor was obtained easily and rapidly. The PSMC sensing probe behavior was studied by measuring, in real-time, temperature changes in water and in air environments. In water environment experiments, the performance of the PSMC sensing probe was characterized, obtaining a sensitivity around 110 pm/ºC and a resolution in the 10^{-4} ºC range. In air environment experiments, it was observed that, first, for equal temperature changes, higher noise levels were measured at higher temperatures due to the temperature transmission dynamics through the environment and, then, the response was in real-time. In summary, the experiment results obtained in both environments demonstrate that a temperature sensing probe able to measure very small temperature variations in real-time, with a very high resolution and at a very specific point was developed.

In comparison with other FOSs previously reported, our sensor presents a higher sensitivity. Furthermore, due to the fact that the sensing element was the PSMC sensor, the development of the sensing probe was cheaper, faster and easier to carry out.

In conclusion, the reported fiber-optic porous silicon temperature sensing probe constitutes the ideal combination of high-sensitivity, easy, rapid and low-cost fabrication and real-time response.

References

1. J. Lou, Y. Wang, and L. Tong, "Microfiber optical sensors: A review," *Sensors*, vol. 14, pp. 5823–5844, 2014.
2. B. Lee, "Review of the present status of optical fiber sensors," *Opt. Fiber Technol.*, vol. 9, pp. 57–79, Apr-2003.
3. A. D. Kersey, "A Review of Recent Developments in Fiber Optic Sensor Technology," *Opt. Fiber Technol*., vol. 2, pp. 291–317, 1996.
4. K. T. V Grattan and T. Sun, "Fiber optic sensor technology: An overview," *Sensors Actuators, App. Phys.*, vol. 82, pp. 40–61, 2000.
5. S. W. Harun, M. Yasin, H. A. Rahman, H. Arof and H. Ahmad, "Fiber Optic Temperature Sensors," in *Optical Fiber Communications and Devices*, InTech, pp. 361–380, 2012.
6. P. Lu, L. Men, K. Sooley, and Q. Chen, "Tapered fiber Mach-Zehnder interferometer for simultaneous measurement of refractive index and temperature," *Appl. Phys. Lett*., vol. 94, pp. 2007–2010, 2009.
7. C. I. Merzbacher, A. D. Kersey, and E. J. Friebele, "Fiber optic sensors in concrete structures: a review," *Smart Mater. Struct*., vol. 5, pp. 196–208, 1996.
8. H. Ahmad *et al*., "High Sensitivity Fiber Bragg Grating Pressure Sensor Using Thin Metal Diaphragm," *IEEE Sensors J.*, vol. 9, no. 12, pp. 1654–1659, 2009.
9. G. Liu, M. Han, and W. Hou, "High-resolution and fast-response fiber-optic temperature sensor using silicon Fabry-Pérot cavity," *Opt. Exp*., vol. 23, pp. 7237–7247, 2015.
10. D. Zhang, J. Wang, Y. Wang, and X. Dai, "A fast response temperature sensor based on fiber Bragg grating", *Meas. Sci. Technol*., vol. 25, no. 7, 2014.
11. L. V. Nguyen, D. Hwang, S. Moon, D. S. Moon, and Y. Chung, "High temperature fiber sensor with high sensitivity based on core diameter mismatch," *Opt. Express*, vol. 16, no. 15, p. 11369, 2008.
12. S. W. James and R. P. Tatam, "Optical fibre long-period grating sensors: Characteristics and application," *Meas. Sci. Technol.*, vol. 14, no. 5, 2003.
13. P. Granitzer and K. Rumpf, "Porous silicon-a versatile host material," *Materials*, vol. 3, pp. 943–998, 2010.
14. O. Bisi, S. Ossicini, and L. Pavesi, "Porous silicon: A quantum sponge structure for silicon based optoelectronics," *Surf. Sci. Rep.*, vol. 38, no. 1, pp. 1–126, 2000.
15. F. A. Harraz, "Porous silicon chemical sensors and biosensors: A review," *Sensors Actuators, B Chem.*, vol. 202, pp. 897–912, 2014.
16. A. Jane, R. Dronov, A. Hodges, and N. H. Voelcker, "Porous silicon biosensors on the advance," *Trends Biotechnol*., vol. 27, no. 4, pp. 230–239, 2009.
17. Y. Zhao, G. Gaur, S. T. Retterer, P. E. Laibinis, and S. M. Weiss, "Flow-Through Porous Silicon Membranes for Real-Time Label-Free Biosensing," *Anal. Chem.*, vol. 88, no. 22, pp. 10940–10948, 2016.
18. L. De Stefano *et al.*, "Porous silicon-based optical biochips," *J. Opt. A Pure Appl. Opt.*, vol. 8, no. 7, pp. S540–S544, 2006.
19. S. Mariani, L. Pino, L. M. Strambini, L. Tedeschi, and G. Barillaro, "10 000-Fold Improvement in Protein Detection Using Nanostructured Porous Silicon Interferometric Aptasensors," *ACS Sensors*, vol. 1, no. 12, pp. 1471–1479, 2016.
20. P. A. Snow, E. K. Squire, P. S. J. Russell, and L. T. Canham, "Vapor sensing using the optical properties of porous silicon Bragg mirrors," *J. Appl. Phys.*, vol. 86, no. 4, pp. 1781–1784, 1999.
21. I. Rendina, I. Rea, L. Rotiroti, and L. De Stefano, "Porous silicon-based optical biosensors and biochips," *Phys. E Low-Dimensional Syst. Nanostructures*, vol. 38, no. 1–2, pp. 188–192, 2007.
22. R. Caroselli, D. Martín Sánchez, S. Ponce Alcántara, F. Prats Quilez, L. Torrijos Morán, and J. García-Rupérez, "Real-Time and In-Flow Sensing Using a High Sensitivity Porous Silicon Microcavity-Based Sensor," *Sensors*, vol. 17, no. 12, p. 2813, 2017.
23. M. A. Anderson *et al.*, "Sensitivity of the optical properties of porous silicon layers to the refractive index of liquid in the pores," *Phys. Status Solidi*, vol. 197, no. 2, pp. 528–533, 2003.
24. P. Li *et al.*, "Spectrometer-free biological detection method using porous silicon microcavity devices," *Opt. Express*, vol. 23, no. 19, p. 24626, 2015.
25. K. Kim and T. E. Murphy, "Porous silicon integrated Mach-Zehnder interferometer waveguide for biological and chemical sensing," Opt. Express, vol. 21, no. 17, p. 19488, 2013.
26. G. A. Rodriguez, S. Hu, and S. M. Weiss, "Porous silicon ring resonator for compact, high sensitivity biosensing applications," *Opt. Express*, vol. 23, no. 6, p. 7111, 2015.

27. R. Caroselli *et al.*, "Experimental study of the sensitivity of a porous silicon ring resonator sensor using continuous in-flow measurements," *Opt. Express*, vol. 25, no. 25, pp. 1781–1784, 2017.
28. Ryan B. Balili, "Transfer matrix method in nanophotonics," *Int. J. Mod. Phys. Conf. Ser.*, vol. 17, pp. 159-168 (2012).
29. L. Pavesi, "Porous silicon dielectric multilayers and microcavities," *Rivista del Nuovo Cimento*, vol. 20, pp. 1-76 (1997).
30. D.A.G. Bruggeman, "Dielectric constant and conductivity of mixtures of isotropic materials," *Ann. Phys.*, vol. 24, p. 636-679 (1935).